Title
Measurement of amplification and absorption of a THz quantum-cascade metasurface free-space amplifier

Journal
AIP Advances, 12(11)

ISSN
2158-3226

Authors
Curwen, Christopher A
Shahili, Mohammad
Addamane, Sadhvikas J
et al.

Publication Date
2022-11-01

DOI
10.1063/5.0122154

Measurement of amplification and absorption of a THz quantum-cascade metasurface free-space amplifier

Christopher A. Curwen,[1,a)] Mohammad Shahili,[2] Sadhvikas J. Addamane,[3] John L. Reno,[3] Boris S. Karasik[1], Benjamin S. Williams[2], and Jonathan H. Kawamura[1]

[1]*Jet Propulsion Laboratory, California Institute of Technology, Pasadena, CA 91109, USA.*
[2]*Department of Electrical and Computer Engineering, University of California, Los Angeles, California 90095, USA.*
[3]*Sandia National Laboratories, Center of Integrated Nanotechnologies, MS 1303, Albuquerque, New Mexico 87185, USA.*

a) Author to whom correspondence should be addressed: chris.a.curwen@jpl.nasa.gov

An active amplifying metasurface based on quantum-cascade gain material at 2.7 THz is studied. The metasurface is fist evaluated as the active component of an external cavity laser with excellent beam quality and frequency tunability from 2.55 – 2.8 THz. Amplification and absorption of the metasurface alone is then separately measured at a single frequency using a probe signal from a CO_2-pumped gas laser operating at 2.743 THz. The metasurface reflectance versus bias is measured and compared with expectations from non-equilibrium Green's function simulations of the quantum-cascade gain material, and FEM simulations of the metasurface reflectance. A peak amplification on the order of 0.3 dB is measured. Design strategies are discussed for increasing single-reflection amplification (upwards of 10 dB) and reducing power dissipation. Further increased amplification could be achieved by cascading multiple metasurfaces.

THE MANUSCRIPT

I. Introduction: Metasurfaces based on arrays of metal-metal waveguide cavities have attracted interest in the THz and infrared communities owing to their ability to efficiently couple free-space radiation to subwavelength quantum systems in semiconductor materials. For example, such metasurfaces have been used to develop quantum-well infrared photodetectors (QWIPs) [1, 2], to study strong light-matter coupling with intersubband electronic excitations [3, 4], and to provide enhanced optical nonlinearity [5]. By loading metasurface elements with quantum-cascade (QC) gain material, surface-coupled THz amplifiers [6] and lasers have been demonstrated [7, 8]. One line of work that has seen recent success is the THz QC vertical-external-cavity surface-emitting-laser (QC-VECSEL) [9, 10]. The QC-VECSEL uses a surface-coupled amplifying, reflective metasurface in combination with an external mirror to form an external cavity laser. The large radiating area of the metasurface supports a fundamental Gaussian cavity mode with excellent beam quality. The lasing frequency is determined by the length of the external cavity, and because the metasurface has a broad amplification bandwidth, the lasing frequency can be tuned over a wide frequency range by mechanically adjusting the length of the external cavity [11].

While there are several demonstrations of QC-VECSELs, so far there has been no unambiguous measurement of amplification from the underlying metasurfaces. Such standalone metasurfaces can be of interest for a variety of applications beyond their use in lasers. For example, the simple surface coupling scheme, low quality factor, and broadband response make such metasurfaces a good platform for studying the properties of the underlying QC-material. Alternatively, by increasing the quality factor, such metasurfaces could be utilized as THz amplifiers or modulators. One such metasurface has been studied using THz time-domain-spectroscopy, but limitations in the experimental setup prevented direct measurement of amplification [12]. Here, we present a measurement of the absolute THz absorption (reflectance less than unity) and amplification (reflection greater than unity) of a metasurface as a function of bias on the device, and compare it to expectation based on simulation of the QC-gain material. Additionally, we present design strategies for increasing metasurface amplification. While there are several examples of THz amplifiers using QC gain material, most are edge-coupled ridge waveguide devices with wavelength scale facets that have poor coupling to free space [13-15]. The key advantage of the metasurface approach is that the large radiating aperture can easily and efficiently couple to external free-space signals.

II. Metasurface design: The metasurface design used in this experiment is presented in Fig. 1. It consists of a 1-D array of narrow metal-metal ridge waveguides loaded with THz QC-gain material. The TM_{01} cutoff resonance of the ridges couples to surface radiation in the same manner as a patch antenna, i.e., the antisymmetric fringing electric-fields at the sidewalls of the ridge, which correspond to in-phase equivalent magnetic current sources. The resonant frequency of the metasurface is determined by the width of the ridges, and the peak reflectance at resonance is given by $R = (Q_{rad} - Q_{mat})^2/(Q_{rad} + Q_{mat})^2$, where Q_{rad} is the radiative quality factor and Q_{mat} is a "material" quality factors that contains both losses (metallic and semiconductor) and the effect of QC gain. In the vicinity of transparency ($R = 1$), the reflectance can be approximated as $R = e^{\xi(g-g_{tr})}$, where g_{tr} [cm^{-1}] is the transparency gain coefficient (i.e. the gain coefficient needed to bring the metasurface reflectance to unity), and $\xi(\nu)$ [cm] can be considered an effective interaction length (which contains the lineshape information of the metasurface). The total quality factor of the reflectance spectrum is given by $Q_{tot}^{-1} = Q_{rad}^{-1} + Q_{mat}^{-1}$. $Q_{mat} = \omega_0 n/(g_{tr} - g)c$, where ω_0 is the centre frequency, n is the refractive index of the QC material, g is the applied QC gain coefficient [cm^{-1}], and c is the speed of light. In this model, we have used a frequency independent QC gain coefficient to isolate the properties of the metasurface from the lineshape of the underlying QC material.

The FEM simulated reflectance spectrum of the 1-D ridge-waveguide array used in this study is plotted as a function of frequency in Fig. 1. The metasurface is designed to operate at 2.7 THz, has ridge widths w = 14.2 μm, and a periodicity of 85 μm. Metal and semiconductor losses are included via Drude model, and the QC-gain is modelled with a flat gain spectrum. The radiative losses of such a ridge array are large compared to the material gain/loss, resulting in $Q_{rad} \ll Q_{mat}$. This results in low peak reflectance, and broad spectral response (low Q_{tot}). When building VECSELs, this is an ideal metasurface design because the low amplification can be compensated with stronger external feedback (higher reflectance mirror), while the broad bandwidth allows for broadband frequency tuning. Conversely, the peak amplification can be increased by reducing Q_{rad}, at the expense of bandwidth.

III. Experimental results: We initially characterized the metasurface by building a frequency-tunable VECSEL, as described in Ref. [11]. The total metasurface area was 2×2 mm^2, but only a central 0.9 mm diameter area was electrically biased. The QC-gain material design is identical to that in Ref. [16] (based on design in [17]), and is 10 µm thick. Feedback is provided by a partially reflecting planar mirror fabricated by depositing a metal mesh on a 500 µm thick Z-cut crystal quartz substrate. The mirror has nearly flat reflectance of >99% across the metasurface bandwidth. The lasing frequency of the VECSEL is tuned by mounting the feedback mirror on a translational piezoelectric stage. In Fig. 2(a), the current-voltage-power characteristics are plotted, as well as the lasing frequency and threshold current as a function of cavity length. The device was held at a heat-sink temperature of 77 K (liquid nitrogen), and operated in pulsed mode (10 kHz rep-rate and 1 µs pulses). The lasing frequency was tuned from 2.55 – 2.8 THz (Fig. 2(b)), corresponding to cavity lengths from ~350 – 400 µm. The frequency tuning range was limited by the free-spectral range of the external cavity, which results in hopping as the mode closest to the amplification peak changes. The apparent resonant frequency of the metasurface is ~2.67 THz (centre of the tuning range). This centre frequency should be determined by design of the ridge width, but imperfect lithography and misalignment of the QC gain spectrum can cause slight deviations in the centre frequency.

In Fig. 2(c), the THz signal strength is plotted as a function of duty cycle / pulse width. The metasurface was biased at a rep-rate of 100 Hz, and the pulse width was varied. At longer pulse widths, the output power deviates significantly from the ideal linear increase, suggesting that heating of the device is causing a significant reduction in the QC-gain. Above 0.7 ms pulse widths (7% duty cycle), the average power in fact decreases with increasing pulse width as a result of the input power increasing the average temperature of the heat sink, reducing output power at all times within

the pulse. No lasing was observed with the metasurface was DC biased. Single ridge waveguide devices fabricated simultaneously with the metasurface but dissipating much smaller power operated in continuous wave up to 100 K, which suggests the metasurface could operate in continuous bias if the area or fill factor were reduced.

The experimental setup for measuring the metasurface's amplification is shown in Fig. 3(a). A CH_2F_2 far-infrared gas laser operating at 2.743 THz was used as the signal source [18]. The signal was focused at normal incidence on the metasurface using an off-axis parabolic mirror with a 2-inch focal length, and a portion of the reflected signal was picked-off with a 12 μm thick Mylar beam splitter to be and detected with a silicon bolometer (note that there is no output coupler when using the metasurface as a stand-alone amplifier). Using a pinhole, the spot size of the focused signal was estimated to be <0.75 mm, small enough to fit in the 0.9 mm diameter bias area of the metasurface. The gas laser produces ~5 mW of THz power, but was attenuated to ~200 μW using a lossy material to prevent feedback from the setup, which was observed to destabilize the laser power and frequency. Low excitation power also ensures the metasurface amplifier will not be saturated. The beam was polarized orthogonal to the length of the ridges for optimal coupling (x-axis, as defined in Fig. 1).

The gas laser source was optically chopped at 100 Hz with a 10% duty cycle, and the metasurface biasing was synchronized with the chopping of the source. As indicated by the data in Fig. 2(c), this is a non-optimal biasing condition for maximum metasurface amplification, but pulse width and rep-rate were limited by the size of the beam from the gas laser and the speed of the chopper motor. In Fig. 3(c), amplification of the metasurface is plotted as a function of the electrical bias applied to the metasurface. Absolute amplification values were determined by referencing the reflected signal from an area (~1×3 mm^2) of metallization on the metasurface die, directly adjacent to the metasurface (Fig. 3(b)). The metasurface dewar was mounted on a translational stage to move between the metasurface and the reference area.

The measured metasurface reflection as a function of bias is plotted in Fig. 3(c). At low bias, the metasurface initially shows an increase in absorption at ~6 V. Unity reflectance is observed at ~12 V, which is slightly below the observed threshold of the VECSEL, and a maximum amplification of up to ~0.3 dB is observed at ~13 V. As expected, amplification is observed in the same bias range where lasing is observed when the metasurface is mounted in the VECSEL configuration. Based on the assumption that the metasurface resonance is centred around 2.67 THz (data from Fig. 2(b)), FEM simulation suggest a gain coefficient of 13 cm^{-1} is present in order to achieve the measured

amplification at the signal frequency of 2.743 THz. Due to possible misalignment during translation from metasurface to reference area, oxidation of the copper reference area, and the fact that the excitation beam was comparable in size to the metasurface bias area and reference area, there may be some error in the absolute amplification (hence the use of one significant figure), but the trend versus bias, expectation from simulation, and alignment of transparency and amplification with the lasing region of the VECSEL are indicative of a relatively accurate measurement. At lower temperatures, and shorter pulse widths, the gain and amplification should be larger.

For comparison, non-equilibrium Green's function simulations (NextNano NEGF) of the active region have been performed. The simulated gain/absorption at 2.743 THz as a function of bias is plotted in Fig. 3(d), and shows good qualitative agreement with the measured result, though the simulation shows a weaker absorption feature, and a stronger amplification feature. The difference between the simulated and measured device bias is likely due to extra voltage drop across the metal-semiconductor contacts. In Fig. 3(e), the full simulated gain spectrum of the active region is plotted at select bias points, and in Fig. 3(f) and (g), the band diagram of the active region is plotted at 40 mV/module (peak absorption) and 52 mV/module (peak amplification), respectively. The absorption at 20 mV/module is likely associated with states 3 (blue) and 5 (purple), which have an energy separation of 11.2 meV = 2.71 THz. The specific layer sequence for a single module (in Å, GaAs/**$Al_{0.15}Ga_{0.45}As$**) is 106/**20**/106/**37**/88/**40**/<u>172</u>/**51**. The middle 88 Å of the underlined well is Si-doped at 5×10^{16} cm^{-3} (wafer number VA1034).

IV. Towards higher amplification: One application of particular interest for active THz metasurfaces is their use as THz amplifiers, a novel technology that is largely unavailable. However, a practical amplifier will require higher amplification than the 0.3 dB measured from the current metasurface. In Fig. 4 and Table 1, we summarize three basic strategies to increase metasurface amplification: 1) utilizing thinner QC-gain material, 2) utilizing metasurfaces with patch arrays, rather than ridge arrays, and 3) operating on a higher-order transverse resonance. In all cases, the mechanism of higher amplification is reduced radiative loss compared to stored energy, resulting in higher Q_{rad}. Combining all three factors, the simulation indicates the amplification of a metasurface could increase to 10 dB. Additionally, utilizing thinner active regions [16] and patch designs [19] reduces the device bias and spatial fill factor of gain material across the metasurface, respectively, so the power dissipation per area decreases simultaneously as amplification increases, allowing for larger, more efficient metasurfaces. This can be described as an increase in the collection area of each meta-element [20].

The trade-off of increasing amplification by increasing Q_{rad} is that the metasurface bandwidth is reduced. Additionally, as the gain from the QC material increases, Q_{mat} eventually becomes negative, causing Q_{tot} to increase, also narrowing the bandwidth. Around transparency (amplification of 0 dB), Q_{mat} is very large, and $Q_{tot} \approx Q_{rad}$. At the other extreme, if gain is increased such that $Q_{mat} = -Q_{rad}$, Q_{tot} goes to infinity, the bandwidth reduces to zero, and the metasurface would act as an oscillator rather than an amplifier [6, 8]. In Fig. 4(b), the ratio of Q_{tot}/Q_{rad} is plotted as a function of metasurface amplification. The same curve applies to any metasurface, but broader band metasurfaces require larger QC gain coefficient to achieve a given metasurface amplification. For example, if the QC material has a maximum gain coefficient of 20 cm^{-1}, Fig. 4(b) indicates that 10 dB of amplification could be achieved with a 5 μm thick TM_{030} patch metasurface, Fig. 4(d) indicates that $Q_{tot} \approx Q_{rad}/2$ at 10 dB amplification, and Table 1 indicates that the metasurface has a $Q_{rad} = 280$, so $Q_{tot} \approx 560$, which corresponds to a 3 dB FWHM of ~5 GHz for an amplifier centred at 3 THz (note: Q_{tot} can be larger than Q_{rad} because Q_{mat} is negative). However, experimental studies suggest QC material gain can be upwards of 40 cm^{-1} [21], in which case Fig. 4(b) indicates that 10 dB amplification can be achieved with a 5 μm thick TM_{010} patch metasurface, and Table 1 indicates $Q_{tot} \approx 170$, corresponding to a bandwidth of ~ 18 GHz.

Conclusion: We have demonstrated measurement of 0.3 dB absolute amplification at 2.743 THz from an active metasurface loaded with quantum-cascade gain material, and presented design strategies for optimization of metasurface amplifiers for higher amplification and lower power dissipation to enable DC biasing. Essentially any Q_{rad} can be engineered for the metasurface. The design for a given application depends on the amount of gain available from the QC-material, desired amplification, desired spectral bandwidth, and thermal limitations. In addition to a single amplifying surface, it is possible to consider cascading multiple metasurfaces to achieve either higher amplification, or larger bandwidth.

ACKNOWLEDGMENTS

This research was carried out in part at the Jet Propulsion Laboratory, California Institute of Technology, under a contract with the National Aeronautics and Space Administration. Partial funding was provided by the National Aeronautics and Space Administration (80NSSC19K0700). M. Shahili acknowledges support from a NDSEG fellowship. Microfabrication was performed at the UCLA Nanoelectronics Research Facility. This work was performed, in part, at the Center for Integrated Nanotechnologies, an Office of Science User Facility operated for the

U.S. Department of Energy (DOE) Office of Science. Sandia National Laboratories is a multimission laboratory managed and operated by National Technology and Engineering Solution of Sandia, LLC., a wholly owned subsidiary of Honeywell International, Inc., for the U.S. Department of Energy's National Nuclear Security Administration under contract DE-NA-0003525.

AUTHOR DECLARATIONS

The authors have no conflicts to disclose

DATA AVAILABILITY STATEMENT

The data that supports the findings of this study are available within the article.

REFERENCES

[1] D. Palaferri *, et al.*, "Room-temperature nine-µm-wavelength photodetectors and GHz-frequency heterodyne receivers," *Nature* (2018).
[2] D. Palaferri *, et al.*, "Noise characterization of patch antenna THz photodetectors," *Appl. Phys. Lett.* (2018).
[3] Y. Todorov *, et al.*, "Polaritonic spectroscopy of intersubband transitions," *Phys. Rev. B* (2012).
[4] M. Jeannin *, et al.*, "Ultrastrong Light-Matter Coupling in Deeply Subwavelength THz LC Resonators," *ACS Photonics* (2019).
[5] J. Lee *, et al.*, "Giant nonlinear response from plasmonic metasurfaces coupled to intersubband transitions," *Nature* (2014).
[6] T. Y. Kao *, et al.*, "Amplifiers of free-space terahertz radiation," *Optica* (2017).
[7] T. Y. Kao *, et al.*, "Phase-locked laser arrays through global antenna mutual coupling," *Nat. Photon.* (2016).
[8] J. Perez-Urquizo *, et al.*, "Monolithic Patch-Antenna THz Lasers with Extremely Low Beam Divergence and Polarization Control," *ACS Photonics* (2021).
[9] L. Y. Xu *, et al.*, "Metasurface external cavity laser," *Appl. Phys. Lett.* (2015).
[10] L. Y. Xu *, et al.*, "Terahertz metasurface quantum-cascade VECSELs: theory and performance," *IEEE J. Sel. Top. Quantum Electron.* (2017).
[11] C. A. Curwen *, et al.*, "Broadband continuous single-mode tuning of a short-cavity quantum-cascade VECSEL," *Nat. Photon.* (2019).
[12] Y. Shen *, et al.*, "THz time-domain characterization of amplifying quantum-cascade metasurface," *Appl. Phys. Lett.* (2021).
[13] C. Mauro *, et al.*, "Amplification of terahertz radiation in quantum cascade structures," *J. Appl. Phys.* (2007).
[14] N. Jukam *, et al.*, "Terahertz amplifier based on gain switching in a quantum cascade laser," *Nat. Photon.* (2009).
[15] Y. Ren *, et al.*, "Single mode terahertz quantum cascade amplifier," *Appl. Phys. Lett.* (2014).
[16] C. A. Curwen *, et al.*, "Thin THz QCL active regions for improved continuous-wave operating temperature," *AIP Adv.* (2021).

[17] M. I. Amanti *, et al.*, "Bound-to-continuum terahertz quantum cascade laser with a single-quantum-well phonon extraction/injection stage," *New J. Phys.* (2009).

[18] F. R. Petersen *, et al.*, "Frequencies of CW FIR Laser Lines from Optically Pumped CH_2F_2," *Int. J. Infrared Millim. Waves* (1980).

[19] C. A. Curwen *, et al.*, "Terahertz quantum-cascade patch-antenna VECSEL with low power dissipation," *Appl. Phys. Lett.* (2020).

[20] D. Palaferri *, et al.*, "Ultra-subwavelength resonators for high temperature high performance quantum detectors," *New J. Phys.* (2016).

[21] D. Burghoff *, et al.*, "Dispersion dynamics of quantum cascade lasers," *Optica* (2016).

TABLES

Table 1. Summary of metasurface design parameters.

Design	g_{tr} (cm^{-1})	Q_{rad}	ξ (mm)	Fill-factor
10 μm, ridge	7	14	0.23	16.5%
5 μm, ridge	13.1	27	0.45	17%
5 μm, TM_{010}	16.7	85	1.4	2.8%
5 μm, TM_{030}	14.9	280	5	8.5%

FIGURE CAPTIONS

FIG 1. FEM simulations of metasurface amplification/absorption spectrum as a function of QC material gain. Insets show metasurface geometry and simulation field plots.

FIG 2. QC-VECSEL pulse-mode lasing characteristics at 77 K a) Current-voltage-power curves and beam pattern. b) Threshold current and lasing frequency as the length of the external cavity is tuned. c) Output power vs pulse width (constant rep-rate of 100 Hz).

FIG 3. Metasurface amplification measurement. a) Experimental setup. A1 = attenuator, BS = beam splitter. b) Microscope image of metasurface. c) Measured metasurface reflectance as a function of bias voltage. d) Simulated QC gain/absorption as a function of bias voltage at 2.74 THz. e) Simulated QC gain/absorption spectrum at select bias points. f) Band diagram of QC active region design at 20 mV/module (maximum absorption) and g) 52 mV/module (maximum gain).

FIG 4. Simulations of metasurfaces with higher amplification. a) Areal view of different ridge- and patch-based metasurface geometries. b) Simulated reflectance curves and metasurface parameters. c) Full reflectance curve vs. QC gain for a 5 μm, TM_{030} patch design. d) Bandwidth narrowing as a function of metasurface amplification.

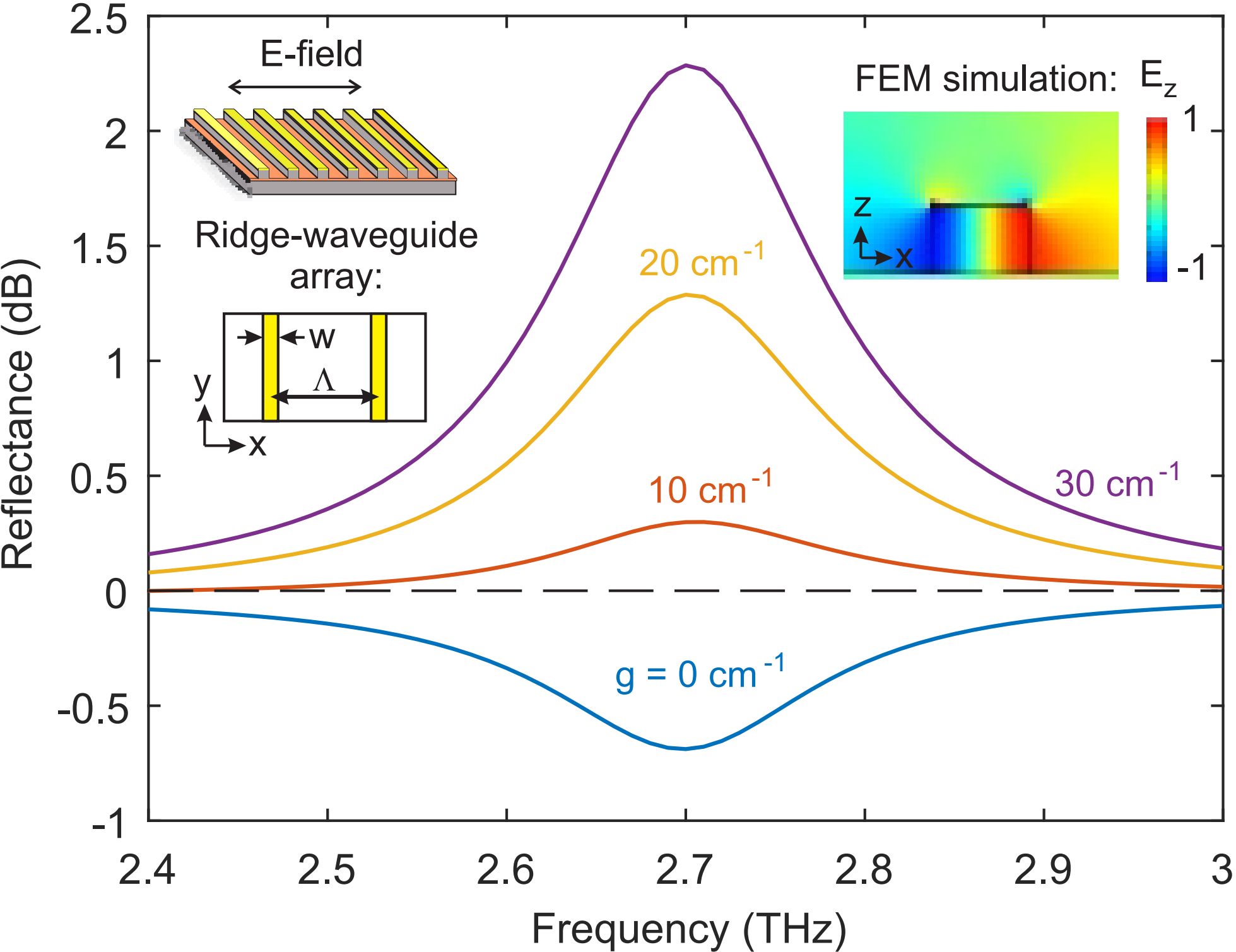
E-field
Ridge-waveguide array:
w
Λ
y
x
FEM simulation: E_z
1
-1
z
x
20 cm^{-1}
10 cm^{-1}
30 cm^{-1}
g = 0 cm^{-1}
Reflectance (dB)
Frequency (THz)
2.5
2
1.5
1
0.5
0
-0.5
-1
2.4
2.5
2.6
2.7
2.8
2.9
3

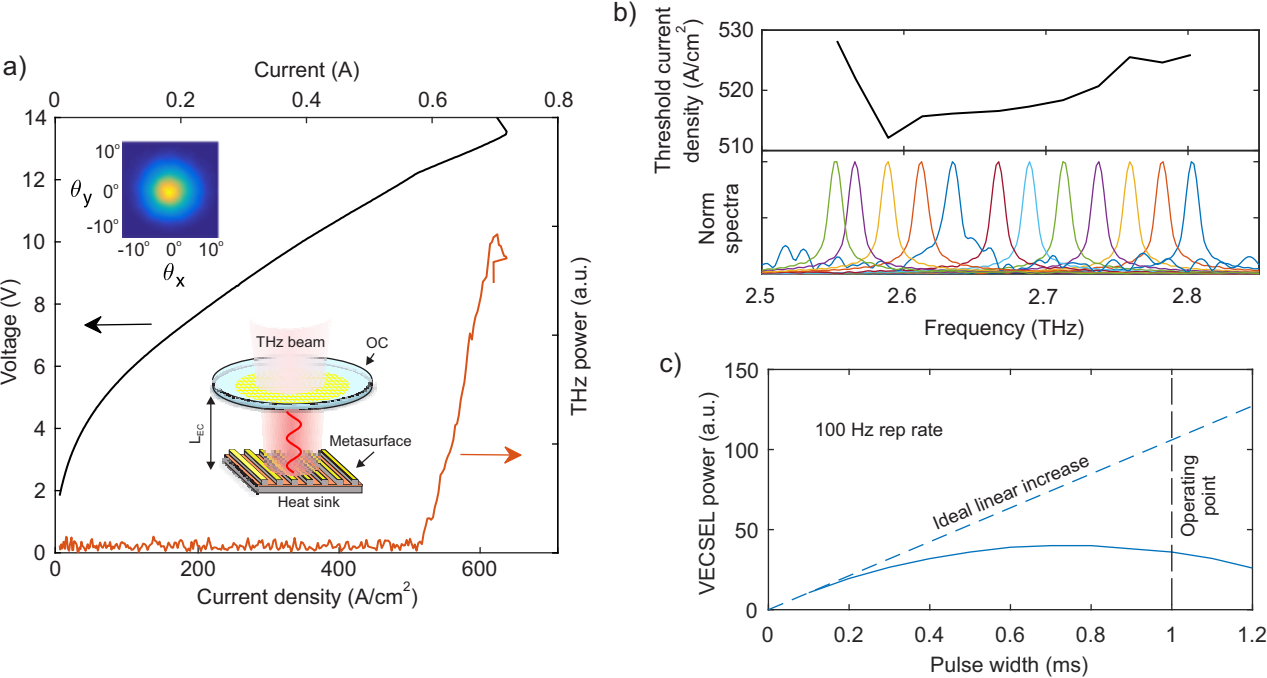
a)
Current (A)
0
0.2
0.4
0.6
0.8
Voltage (V)
THz power (a.u.)
Current density (A/cm^2)
0
200
400
600
θ_y
θ_x
10°
0°
-10°
THz beam
OC
Metasurface
Heat sink
L_{EC}
b)
Threshold current density (A/cm^2)
530
520
510
Norm spectra
2.5
2.6
2.7
2.8
Frequency (THz)
c)
VECSEL power (a.u.)
150
100
50
0
100 Hz rep rate
Ideal linear increase
Operating point
0
0.2
0.4
0.6
0.8
1
1.2
Pulse width (ms)

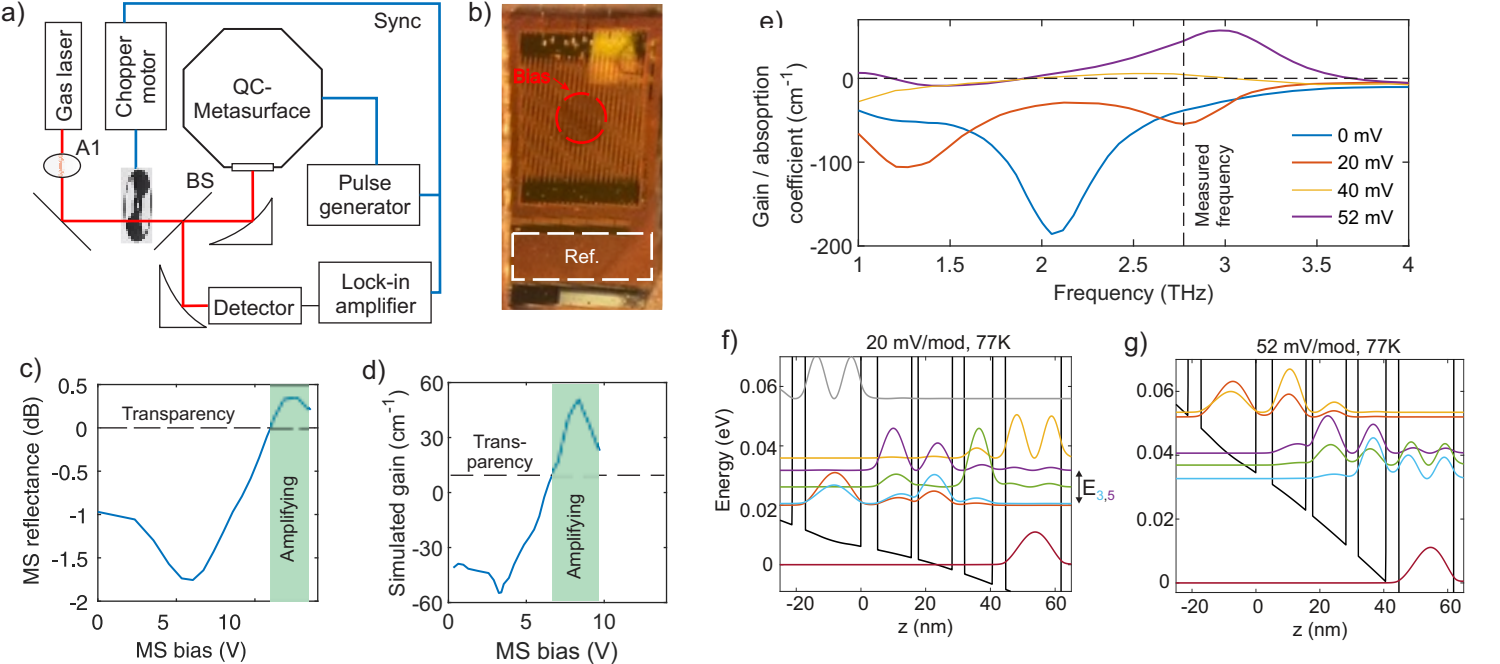
a)
Gas laser
Chopper motor
Sync
QC-Metasurface
A1
BS
Pulse generator
Detector
Lock-in amplifier
b)
Bias
Ref.
e)
Gain / absoprtion coefficient (cm^{-1})
Frequency (THz)
Measured frequency
0 mV
20 mV
40 mV
52 mV
c)
MS reflectance (dB)
Transparency
Amplifying
MS bias (V)
d)
Simulated gain (cm^{-1})
Trans-parency
Amplifying
MS bias (V)
f)
20 mV/mod, 77K
Energy (eV)
$E_{3,5}$
z (nm)
g)
52 mV/mod, 77K
z (nm)

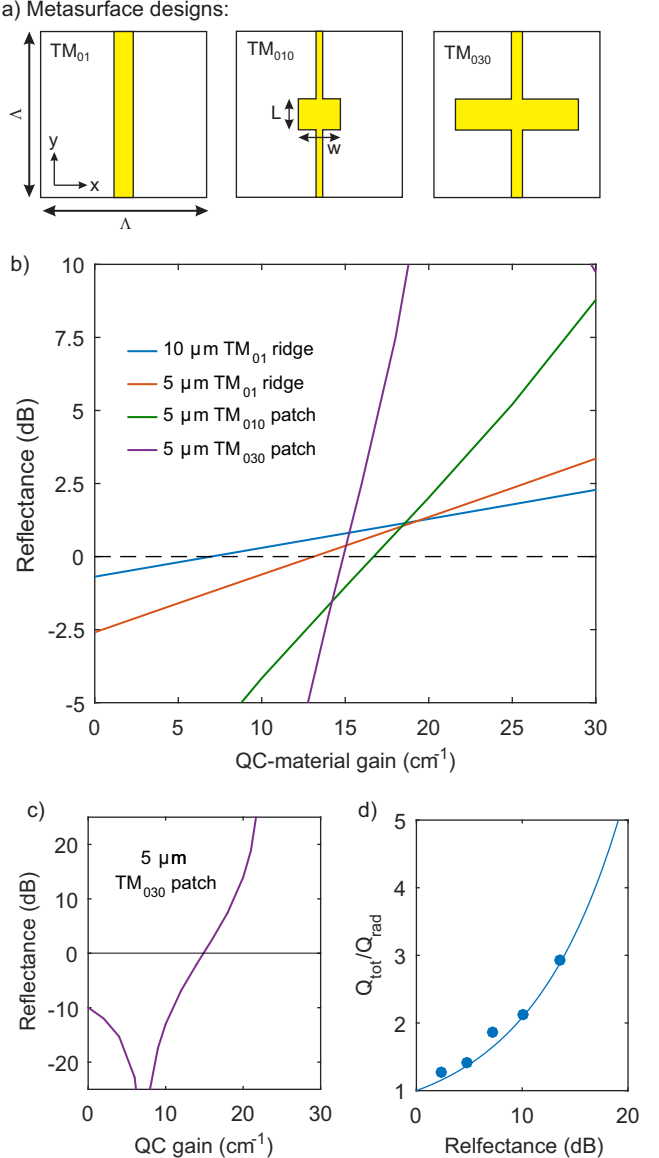
a) Metasurface designs:
TM01
TM010
TM030
L
w
Λ
y
x
b)
10 μm TM01 ridge
5 μm TM01 ridge
5 μm TM010 patch
5 μm TM030 patch
Reflectance (dB)
QC-material gain (cm-1)
c)
5 μm
TM030 patch
Reflectance (dB)
QC gain (cm-1)
d)
Qtot/Qrad
Relfectance (dB)